Journal of Electroceramics 3:2, 143–150, 1999
© 1999 Kluwer Academic Publishers, Boston. Manufactured in The Netherlands.

Ultrasonic Micromotors Based on PZT Thin Films

PAUL MURALT

Laboratoire de Céramique, Swiss Federal Institute of Technology Lausanne, CH-1015 Lausanne, Switzerland

Abstract. The integration of piezoelectric Pb(Zr,Ti)O_3 thin films on silicon substrates for ultrasonic motor applications is reviewed. With suitable buffer and bottom electrode layers the problems due to high processing temperatures in oxygen ambient can be handled. Reproducibility can be increased by stabilized electrode systems and seeding layers for PZT nucleation. Elastic fin micromotors of millimeter size have been fabricated. They achieve the necessary torques, low speeds, and battery voltage operation for applications in wristwatches. However, their efficiency needs to be improved. Better figure of merits of the material still can be achieved. Better designs with larger coupling factors are desirable.

Keywords: ultrasonic actuator, thin films, PZT, integration

1. Introduction

During the recent years, the study of micro-electro-mechanical systems (MEMS) has shown significant opportunities for miniaturized mechanical devices based on silicon technology. Part of the work has been devoted to actuators with the goal to reduce dimensions as required for micro robots, focusing systems for micro optics, and for micro positioning systems needed for example in hard disk drives. Electrostatic, electromagnetic, ultrasonic, thermal and other actuation principles have been demonstrated. Each principle has its strong and weak points. Various aspects need to be considered to gain an overall evaluation of the question which principle is best for a given application. It is not only the theoretically achievable output performance of such a motor which needs to be considered. Suitability for down scaling, realizability of the required structures, and the compatibility with silicon technology are important points as well. It is clear that the last three points may improve considerably with time. Better miniaturized structures will be invented, techniques for micro-machining improve steadily, and advances in materials' processes and materials' compatibility are reported every year. This paper reports on recent advances made in integrating the piezoelectric material $Pb(Zr_xTi_{1-x})O_3$ onto silicon substrates for the fabrication of ultrasonic motors.

As compared to other techniques, ultrasonic actuation bears various strong points. These are the low driving voltages, and the comparatively high torques at low speeds. Torques of 1 μNm at 4 V_{rm}, or 0.3 μNm/V_{rms} have been achieved [1] with millimeter sized rotors. This is much more than what has been demonstrated with electrostatic micromotors (scaled to the same motor size). The low speeds (typically 5 rpm at 2 V_{rms} [1]) of ultrasonic micromotors obliterates the need for gear boxes. These are very difficult to manufacture in submillimeter dimensions, and tend to reduce the output torque to zero because of unsolved friction problems. In some of the applications, as, e.g., for wristwatches, the flat profile of ultrasonic micromotors is an additional advantage. Ultrasonic micromotors have indeed some very attractive features for turning the date wheel of a wristwatch: flatter profiles than today's motors, high enough torques (1 μNm), and low enough supply voltages for battery operation. The disadvantage of ultrasonic micromotors lies in the fact that the coupling between stator and rotor is based on frictional forces, and that there is no constant relation between stator excitation and output speed as with a stepper motor. Complicated phenomena of gliding,

slipping and sticking, of static as well as dynamic friction may happen. However, most of the problems can be solved with a closed loop regulation based on angular position detection [2,3].

For each principle specific technical and materials problems have to be overcome. Whereas for electrostatic rotary micromotors the fabrication control of micron sized air gaps is essential, for ultrasonic micromotors the application of new materials is required. The material which is most widespread in ultrasonic bulk actuators, namely $Pb(Zr,Ti)O_3$, is not compatible with standard silicon technology. For this reason, a number of devices have been fabricated with piezoelectric ZnO thin films [4]. However, considering the size of the relevant thin film $e_{31,f}$ coefficient (see Table 1), it is evident that PZT thin films should yield about ten times higher piezoelectric stresses, which results in higher output torques, or lowering of driving voltages. This indeed has been experimentally confirmed later. PZT thin film driven micromotors of identical design needed 6 to 7 times less voltage for the same torque [2,5]

The early work with PZT thin films suffered from heavy fabrication and deterioration problems. The first demonstrator showing that an object could be rotated by a PZT thin film actuated vibration [11] had a too short lifetime to allow characterization of the operation performance. A number of integration problems needed to be solved first in order to achieve reliable ultrasonic vibrators with PZT thin films [5,12]. Such integration work for MEMS technology consists of two major phases: First the different materials' and the various patterning processes need to be developed in order to meet the requirements of the design, to avoid delamination, and to maintain the functional quality of the applied materials. In a second part, design and dimensions need to be adapted to measured materials properties, and materials have to be optimized. For instance, one has take into account the (unavoidable) mechanical stresses in thin films. In the following, integration issues encountered during the fabrication of ultrasonic micromotors of the ''elastic fin'' type are reviewed, and a critical valuation of the achieved performance is given.

Table 1. Piezoelectric thin film coefficients $e_{31,f}$ [6] compared to derived values from published data of single crystal ZnO [7] and AlN [7], and of ''hard'' bulk ceramic PZT [8]

e_{31} (C/m^2) $e_{31,f}$ [film]	ZnO	AlN	PZT
bulk e_{31}	− 0.37	− 0.58	− 3.6
film: calculated	− 0.68	− 1.05	− 14.7
film: measured	–	− 1.0 [9]	− 8.7 [10]

2. Design of the Ultrasonic Stator

The stators were designed for hybrid versions of ''elastic fin'' micromotors, as depicted in Fig. 1. The motor type was demonstrated with bulk PZT, and proposed for down scaling by Kurosawa et al. [13]. Hybrid refers to the fabrication principle and means in this case that the rotor was fabricated and assembled to the stator by classical means, and that only the stator was obtained with silicon micromachining techniques. This stator consist of a silicon frame keeping a thin silicon membrane which is covered by a PZT thin film. The latter serves to excite standing flexure waves in the membrane. The amplitude of this vibration is proportional to $e_{31,f} \cdot U$, where U is the applied voltage, independently of the thickness of the piezoelectric thin film. The deflections of the membrane are converted into a rotation by a rectifying rotor, which has *tilted* elastic legs or fins. This rectification works in principle as follows: When the membrane moves towards the elastic fins, the latter are compressed and bent. In this phase the fins do not slip because of frictional forces. So the rotor turns in order to release the compression. When the membrane moves away from the fins (decompression) the frictional forces are minimal and the fins glide forward, following the body of the rotor. The

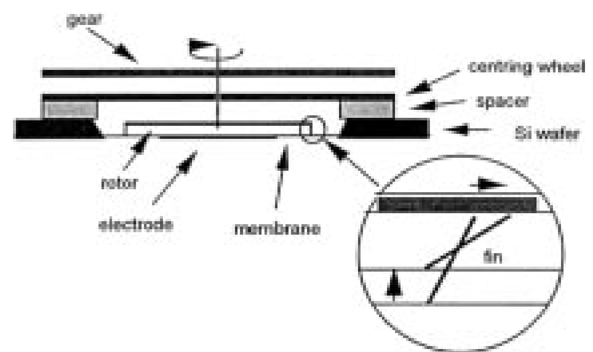

Fig. 1. Hybrid construction of an elastic fin micromotor (from ref. [5]). The silicon wafer is upside-down, the rotor moves inside the etched cavity. The operation principle of the fins is explained in the insert. The normal force between rotor and stator was increased by putting weights onto the gear.

3.5 mm diameter rotor was cut out by laser from a metallic foil. The desired tilt angle of the legs was achieved by molding in a pressing machine. A steel axle of 0.25 mm diameter is clamped into the rotor and centered by a centering wheel resting on spacers. On the top of the axle a wheel was fixed which serves as a load to increase the friction and the moment of inertia for torque measurements.

The first version of the piezoelectric thin film stator was made as simple as possible. The sequence of thin films can be seen in Fig. 2. The piezoelectric film, as well as the ground electrode below, covered the whole membrane. Contact pads, conductor lines and top electrodes were patterned from the same aluminum film, deposited directly on the PZT layer. For this first version, the top electrode just was a round central electrode covering half of the membrane diameter. This was good to excite the ground mode B_{00}, but enabled also the excitation of the B_{10} mode with one circular node (see Fig. 3). The membranes were obtained by bulk micromachining of single crystal silicon wafers, i.e., anisotropic wet etching in hot KOH through a backside mask.

This first design worked well for demonstration purposes and the first characterizations. However, the top electrode design was not optimal for the excitation of the B_{10} mode, the one yielding the largest coupling between stator and rotor (see Fig. 3). In addition, parasitic capacities due to conductor lines and contact pads reduced the electromechanical coupling coefficient k^2 of the ultrasonic stator. For this purpose a second design was elaborated [1,14] (see Fig. 4). This included a silicon dioxide layer on top of the PZT thin

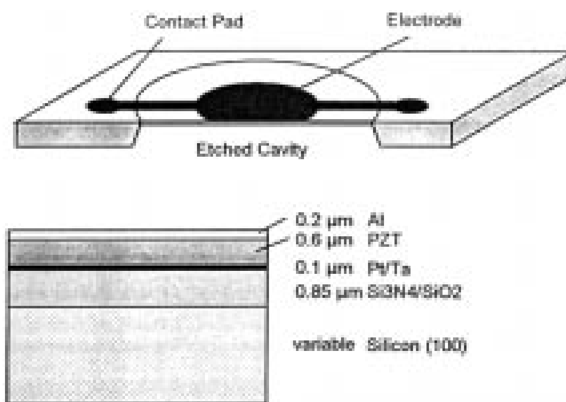

Fig. 2. Schematic structure of the first PZT thin film stator [5].

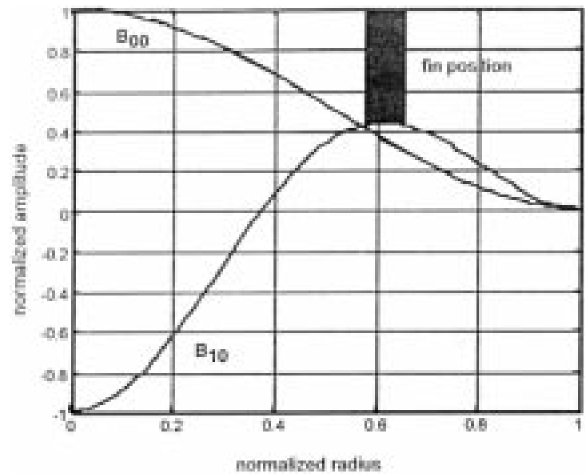

Fig. 3. Deflection as a function of the radius for the two radial modes B_{00} and B_{10}. The ideal position of the rotor fins is indicated.

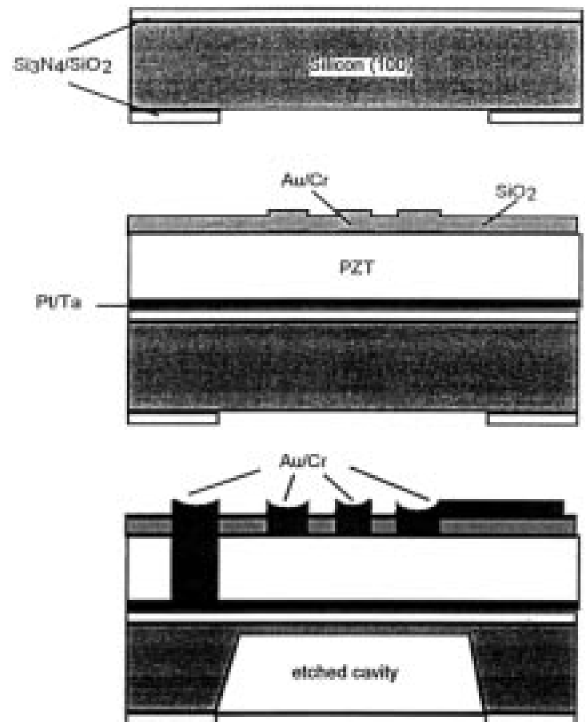

Fig. 4. Schematic structure and major fabrication steps of second design with bottom electrode contact, optimized electrode, and low dielectric SiO_2 layer (according to ref. [1]).

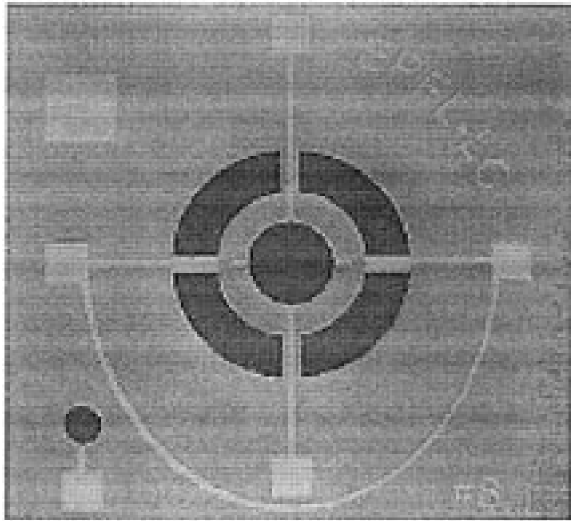

Fig. 5. View onto top electrodes (darker parts) and contact lines and pads (bright). Central and outer electrode have two connections each. The bottom electrode connection is in the lower left corner of the image (from ref. [1]).

film in order to reduce the capacity of conductor lines and contact pads. An electrode system (see Fig. 5) consisting of an annular electrode and a central electrode was shaped to excite accurately the B_{10} mode with two ac voltages having a relative phase shift of 180°.

3. Fabrication

The prime concern is bottom electrode stability against the conditions prevailing during PZT film in-situ growth or crystallization annealing: oxidizing ambient and the presence of lead oxide at high temperatures (550 to 700°C). Degradation of the bottom electrode structure may affect adhesion, PZT properties and electrode conductivity and morphology, while lead oxide can diffuse through the platinum bottom electrode and react with SiO_2 to form silicates [15,16] or compounds with the adhesion layer [17].

Silicon needs to be protected by a buffer layer preventing oxygen and silicon diffusion. The standard choice is SiO_2, i.e., a thermal oxide layer. This was not suitable in our case. For bulk micromachining in KOH, a layer of LPCVD -Si_3N_4 is needed as a masking layer on the backside of the wafer. PECVD nitride, usually deposited at 300°C, does not work, because hydrogen is released during PZT processing. Unfortunately, the LPCVD nitride is deposited on both sides of the wafer. Hence, the nitride layer on the front side becomes a part of the membrane. The high tensile stress in LPCVD nitride of about 1 GPa would lead to fragile membranes, and would also reduce the coupling factor of the membrane stator. Tensile stresses result in stretching forces at the border of the membrane. These reduce the amplitude of vibration of the stator, a transition from disk to thin membrane behavior occurs [12,18]. The reduction of coupling coefficient *k*, and the increase of the vibration frequency can be calculated analytically for round ideal disks (along the theory given in ref. [1]). Figure 6 shows the result for an average film stress of only $+40$ MPa, which already may degrade the coupling factor to half the maximum value. The stress was therefore compensated by growing the nitride on a thermal oxide layer, which is a compressivley stressed layer. With 650 nm of oxide, the stress of 200 nm of nitride was compensated. This combination was actually the same as used for pyroelectric devices [19]. Another solution consists in using (nitrogen deficient) low stress nitride [2], which can be grown up to a thickness of 0.5 μm. The advantage of the bilayer is that it can be purchased

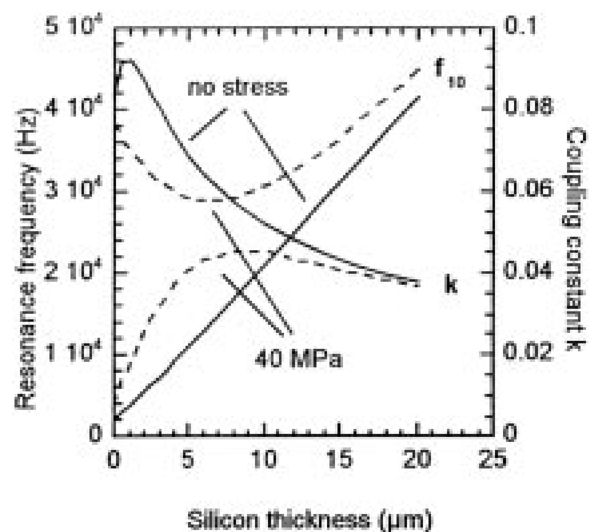

Fig. 6. Calculated coupling factor and eigen frequency as a function of silicon thickness for a round disk of silicon covered by a layer stack, including PZT, as discussed in the text (the calculations base on the theory given in ref. [1]. The calculations are shown for a stress free and a tensile stressed layer stack.

easily from many CMOS facilities. In this case the first fabrication step consists in patterning of the masking layer on the back side for the later KOH etching (as shown in the first schematic of Fig. 3).

The second step was the sputter deposition of the Pt bottom electrode. We tested several adhesion layers between Si_3N_4 and Pt. Among Ti, TiO_2/Ti, Ta, Ta_2O_5/Ta the single Ta layer withstood best the PZT process and the subsequent patterning steps. This is in contrast to the optimal solution on SiO_2, where the pre-annealed TiO_2/Ti [20] is by far the best choice among the above mentioned materials. The different behavior of the adhesion layers on nitride has not been investigated in detail. In a comparative study [17] of stabilized Pt electrodes using Ti, Zr, and Ta adhesion layers it was observed that Ti diffuses through the platinum film, while Zr and Ta stay mostly in place. This behavior originates from the fact that the mobile species are the Ti ions in titania, and the oxygen ions in zirconia and Ta_2O_5. Oxygen thus diffuses rather into the Ta and Zr layer, whereas Ti migrates through the already formed oxide, and through the Pt grain boundaries to react with oxygen. Pockets of TiO_2 have indeed been found between Pt grains (see Fig. 7). The out-diffused Ti leaves nano-pores behind. In addition to oxygen, lead diffuses down into the adhesion layer. One finds a lot of lead in the former Ta layer, which has reacted to pyrochlore with Pb and oxygen (see Fig. 8). Much less lead is found in the former Ta_2O_5 layer and the remaining porous TiO_2 layer. It seems that the lead content in the adhesion layer is rather beneficial for good adhesion on silicon nitride, and

Fig. 7. Platinum electrode on Ti adhesion layer observed by TEM imaging. A TiO_2 pocket is seen the grain boundaries (arrow), as verified by electron energy loss spectroscopy [17].

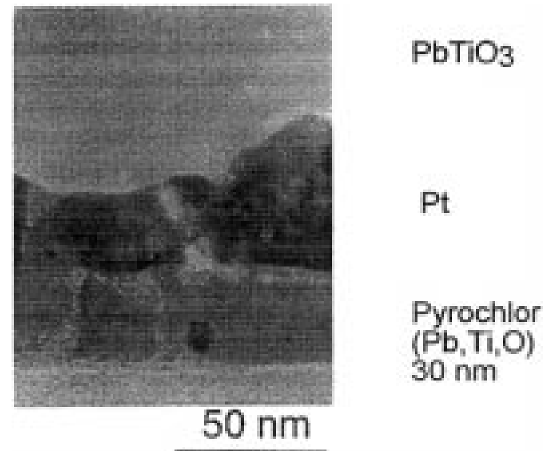

Fig. 8. TEM image of platinum electrode sandwiched between $PbTiO_3$ and Ta layer. After $PbTiO_3$ deposition, the Ta layer is 3 times thicker and transformed to pyrochlore [17].

that the pores in TiO_2 apparently (Ti adhesion layer) are a more serious problem on nitride than on oxide. Delamination during wet etching of the top electrode—or even in the development bath—is caused by fast diffusion of the etchant along the adhesion layer. Additionally, the etchant may attack the adhesion layer through the uncovered Pt layer. The wet etching of aluminum layers, top electrodes or other layers, have been experienced to cause often delamination. This was one of the reasons why the top electrode material has been changed in the second design.

The PZT 53/47 film was deposited by sol-gel and sputter deposition techniques The processes needed maximal temperatures of 600°C (sol gel) and 530°C (sputtering). The sol gel deposition was based on a standard process with the organometallic precursors $Pb(C_2H_4O_2)_2$ $3H_2O$, $Zr(OCH_2CH_2CH_3)_4$ and $Ti[OCH(CH_3)_2]_4$ [21]. The film exhibited a strong <111> texture due to a special heat treatment [22,23]. The sputtered PZT 40/60 with <100> orientation was grown in situ from 3 simultaneously operating magnetrons with metal targets. The orientation was obtained due to a <100> oriented lead titanate template layer of 30 nm thickness, which was deposited previously in the same sequence [24]. In both cases the PZT film was 0.6 μm thick, which was enough for achieving a low voltage operation.

The aluminum top electrode of the first design was deposited by evaporation and structured afterwards. Finally the silicon etching in KOH of the back side was performed. The front side was protected by a

hermetically closed chuck. The membrane thickness of 10 to 50 μm was controlled by the etching time. Figure 9 shows a cross section through a cleaved membrane, as observed by SEM (scanning electron microscopy). For motor operation the wafer was turned up-side down. The rotor was thus moving on the silicon side in the etched cavity (see Fig. 1).

For the improved second design [1], a quartz layer was sputter deposited on the PZT film (see Fig. 10). In a first attempt it was tried to define the electrodes by opening holes through the SiO_2 by reactive ion etching in CF_4 . However, the capacity decreased very much by this procedure. The permittivity was reduced from 850 to typically 400. Although PZT was not etched in the CF_4 plasma, a thin surface layer of low dielectric constant was formed. XPS (y-ray photo-electron spectroscopy) measurements revealed a strongly fluorinated surface [1]. To correct this problem, the sites of the top electrodes were covered with a lift-off patterned Au/Cr protection film before quartz deposition (see Fig. 4, center drawing). The quartz layer was then opened, the protection film was removed, and a new Au/Cr (330/10 nm) top electrode was deposited (see Fig. 11). The contacts to the bottom electrodes were obtained by wet etching of PZT in HCl:HF.

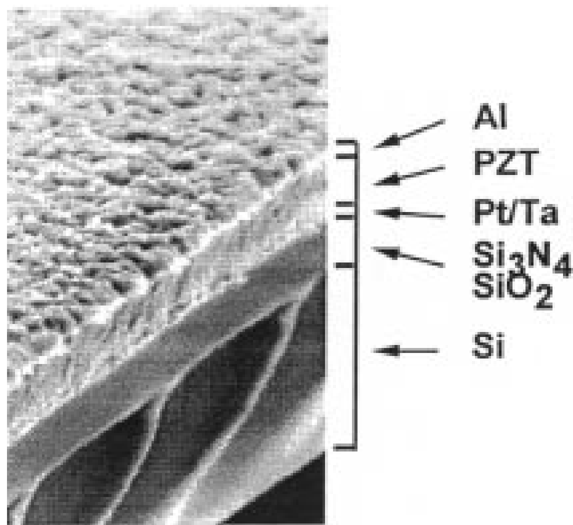

Fig. 9. SEM image of a cleaved stator membrane (from [5]).

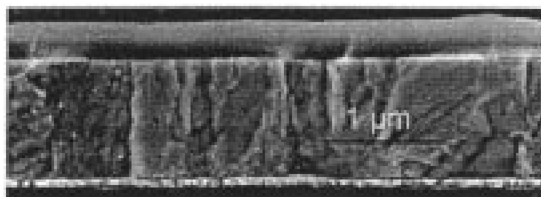

Fig. 10. SEM cross section through the layers sequence SiO_2 (250 nm) on PZT (1 μm) on Pt (100 nm).

4. Materials and Design Improvements

Perfect integration strategies include the controlled nucleation of PZT thin films, because their growth is nucleation controlled. This implies that the bottom electrode is of reproducible quality. Quite often, PZT nucleation relies on the fact that Ti from the adhesion layer diffuses through the platinum during PZT anneal to serve as nucleation centers for PZT [25]. Such diffusion processes may not be very well reproducible. Controlled growth can be obtained on stabilized platinum electrodes of good (111)-texture [17] to which a TiO_2 or Ti seeding layer is added [26,27]. These electrodes normally result in well (111)-textured PZT thin films (see Fig. 12).

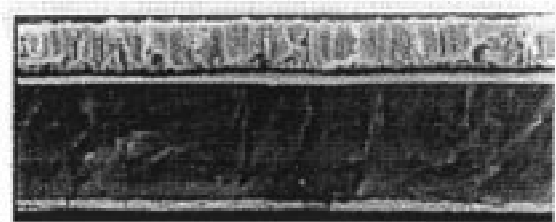

Fig. 11. SEM cross section through the Au/Cr/PZT/Pt layers.

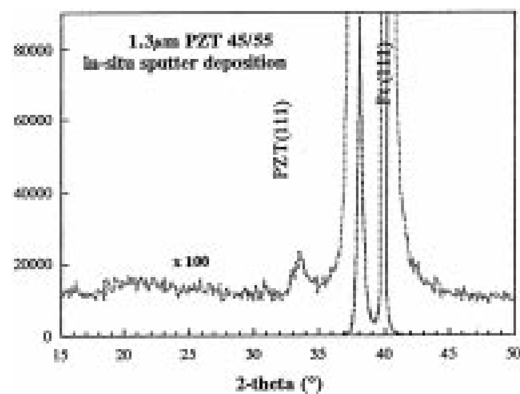

Fig. 12. X-ray Θ-2Θ diffractogram for a 1.3 μm thick (111) textured PZT film grown by sputter deposition and TiO_2 seeding. No other peaks than (111) and higher orders of it can be found.

The study of power consumption by the micromotor [1] showed that the large permittivity of PZT requires careful design of the electrodes. Given that the operation frequency amounts to 20 to 100 kHz, and that the capacity C can amount to several nF, the ac current $J_{rms} = 2\pi f \cdot CU_{rms}$, may become quite large, so that the main power consumption may originate from Joule heating in the electrodes. This can be avoided by having thick enough electrodes and by feeding the power in as closely as possible to the capacitors. Once the resistive losses are removed by an appropriate design, the dielectric losses become apparent. The calculated coupling coefficient of our stator reaches in the best case about $k = 0.1$, or $k^2 = 0.01$ ([1], for $e_{31,f} = 6$ C/m^2). This value is considerably smaller than the dielectric loss tangent, which typically is measured as 0.03. Taking into consideration that only a few percent of the stator power is transmitted to the rotor [1,2] an efficiency below 1% is obtained. It is obvious that the lowering of the dielectric loss is an important issue for ultrasonic applications. The optimization of PZT thin films should take into account the complete figure of merit (FOM) for the desired application, in this case for ultrasonic excitation efficiency.

$$FOM = \frac{e_{31,f}^2}{\varepsilon_r \varepsilon_0 \cdot \tan\delta}$$

Knowledge from bulk ceramics cannot simply be applied for thin films. In bulk ceramics all piezo-

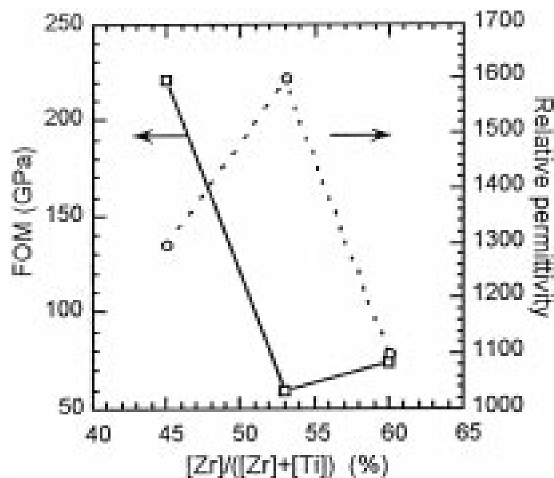

Fig. 13. Materials figure of merit for ultrasonic actuation as a function of PZT composition. The films were grown by chemical solution deposition, were (111)-textured and 1 μm thick [10].

electric coefficients peak at the morphotropic phase boundary. In thin films this is not necessarily the case. A preliminary study yielded the surprising result that the piezoelectric coefficient $e_{31,f}$ does not peak at the same composition as the permittivity (see Fig. 13) [10]. Translated into motor performance, PZT45/55 would yield 70% more power and 360% more efficiency than PZT 53/47. The more, bulk properties indicate that the thin film piezoelectric coefficient might be higher than known today (see Table 1).

Improvements can also be expected from other designs. Estimate calculations show that k^2 of the thin clamped disk is about 5 time smaller than k^2 of a disk fixed in the center only. Of course, it is rather difficult to micro-machined a disk held in the center and having correct electrical connections. However, there might be other designs allowing to raise the coupling coefficient.

In the designs presented above, the stator membrane is mostly composed of ceramic materials. However, metallic membranes or disks would offer some advantages. They are less brittle, and they can carry electrical current and thus allow to decrease the resistance in the bottom electrode. Due to high processing temperatures one is of course restricted to metals with moderate thermal expansion coefficients. In a first study, 1 μm thick membranes of zirconium, coated with PZT have been fabricated and piezoelectric actuation has been demonstrated. [28]. The key point here is to avoid interdiffusion of oxygen and lead from the PZT process with the underlying, strongly reactive Zr layer. It turns out that oxide electrodes such as RuO_2 are much suited for such barrier functions than platinum electrodes. A reactive layer below the RuO_2 is oxidized only as long as the RuO_2 is reduced. This process can be stopped when a material is taken that forms and oxide scale, such as Cr. A working electrode/barrier sequence was thus found with RuO_2/Cr/Zr. The Cr oxide scale enhances the resistance for the current between Zr and RuO_2[29]. However, it is so thin that this resistance is acceptable for ultrasonic applications (see Fig. 14).

5. Summary and Outlook

Integration technology of PZT thin films is advanced enough to fabricate working and reliable micromotors. The technical limits of a present version have been explored. While torque, speed and operation

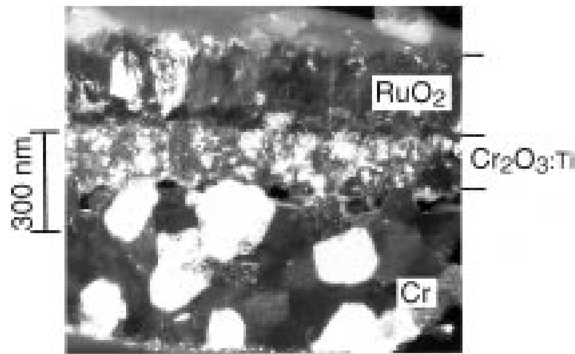

Fig. 14. TEM cross-section of the RuO_2/(Ti)/Cr sequence after a 10 min annealing step in oxygen at 800°C (from ref. [30]).

voltage are in the desired range for watch applications, the efficiency is too small. Improvements are necessary and possible on the materials as well on the design side to increase the coupling coefficient. The PZT thin films still can be improved by choosing the optimal composition. Substitutions, as known from bulk ceramics, need to be checked for lowering the dielectric loss. New vibrating structures as stators, and new rotors are desired for improving the coupling coefficient and also the conversion efficiency between stator and rotor. The evolution of micromachining technology will certainly help to fabricate more complicated and also more precise mechanical structures.

Acknowledgments

The author would like to thank M.-A.Dubois and S.Hiboux for the use of some unpublished figures (SEM photographs X-ray measurements). The work was supported by the Swiss Priority Program on Materials Research and the Swiss Institute of Technology (EPFL) in Lausanne.

References

1. M.-A. Dubois and P. Muralt, *IEEE Trans. UFFC*, **45**, (1998).
2. G.-A. Racine, P. Muralt, and M.-A. Dubois, *Smart Materials and Structures*, **7**, 404 (1998).
3. G.-A. Racine, C. Beuret, R. Luthier, and N.F.de. Rooj, *IEEE Micro Electro Mechanical Systems*, (1994).
4. G.-A. Racine, R. Luthier, and N.F.de. Rooj, *IEEE-MEMS*, (1993).
5. P. Muralt, M. Kohli, T. Maeder, A. Kholkin, K.G. Brooks, N. Setter and R. Luthier, *Sensors and Actuators A*, **48**, 157 (1995).
6. P. Muralt, *J. Int. Ferroelectrics*, **17**, 297 (1997).
7. T. Ikeda, *Fundamentals of piezoelectricity*, Oxford: Oxford University Press (1990).
8. A.J. Moulson and J.M. Herbert, *Electroceramics*, London: Chapman & Hall (1990).
9. M.-A. Dubois and P. Muralt, *Sensors and Actuators A*, in press (1999).
10. M.-A. Dubois, P. Muralt, D.V. Taylor, and S. Hiboux, *Integrated Ferroelectrics*, 22,535 (1998).
11. A.M. Flynn, L.S. Tavrow, S.F. Bart, and R.A. Brooks, *J. Microelectromechanical Systems*, **1**, 44 (1992).
12. P. Muralt, A. Kholkin, M. Kohli, and T. Maeder, *Integrated Ferroelectrics*, **11**, 231 (1995).
13. M. Kurosawa, T. Uchiki, H. Hanada, K. Nakamura, and S. Ueha. *IEEE Ultrasonics Symposium*, (Tuscon 1992).
14. M.A. Dubois, P. Muralt, K.G. Brooks, and R. Luthier. *5th Int. Conf. New Actuators*, (Bremen 1996),
15. P.D. Hren, S.H. Rou, H.N.A. Shareef, and M.S. Ameen, *Integrated Ferroelectrics*, **2**, 311 (1991).
16. L.D. Madsen and L. Weaver, *J. Electron. Materials*, **21**, 93 (1992).
17. T. Maeder, L. Sagalowicz, and P. Muralt, *Jap. J. Appl. Phys.*, **37**, 2007 (1998).
18. P. Muralt, A. Kholkin, M. Kohli, and T. Maeder, *Sensors and Actuators A*, **53**, 397 (1996).
19. M. Kohli, C. Wüthrich, K.G. Brooks, and B. Willing, *Sensors and Actuators A*, **60**, 147 (1997).
20. K. Sreenivas, I. Reaney, T. Maeder, and N. Setter, *J. Appl. Phys.*, **76**, 466 (1994).
21. S.K. Dey, K.D. Budd, and D.A. Payne, *IEEE Trans UFFC*, **35**, 80 (1988).
22. K.G. Brooks, I.A. Reaney, R. Klissurska, and Y. Huang, *J. Mater. Res.*, **9**, 2540 (1994).
23. I.M. Reaney, K.G. Brooks, R. Klissourska, C. Pawlaczyk, and N. Setter, *J. Amer. Cer. Soc.*, **77**, 1209 (1994).
24. T. Maeder, P. Muralt, M. Kohli, A. Kholkin, and N. Setter, *British Ceram. Proc.*, **54**, 206 (1995).
25. G.J. Willems, D.J. Wouters, and H.E. Maes, *Integrated Ferroelectrics*, **15**, 19 (1997).
26. P. Muralt, T. Maeder, L. Sagalowicz, and S. Hiboux, *J. Appl. Phys.*, **83**, 3835 (1998).
27. K. Aoki, Y. Fukuda, K. Numata, and A. Nishimura, *Jpn. J. Appl. Phys.*, **34**, 192 (1995).
28. T. Maeder, P. Muralt, L. Sagalovicz, and I. Reaney, *Appl. Phys. Lett.*, **68**, 776 (1996).
29. T. Maeder, P. Muralt, L. Sagalowicz, and N. Setter, *J. Kor. Phys. Soc.*, **32**, S1569 (1998).